Global Journal of Researches in Engineering: C
Chemical Engineering
Volume 19 Issue 2 Version 1.0 Year 2019
Type: Double Blind Peer Reviewed International Research Journal
Publisher: Global Journals
Online ISSN: 2249-4596 & Print ISSN: 0975-5861

Chemistry Synthesis, Characterization and Photocatalysis of $KSr_2Nb_5O_{15}$ Doped with Nickel

By Paulo César Faria
University of the State of Sao Paulo

Abstract- Potassium and strontium niobate ($KSr_2Nb_5O_{15}$) of tungsten structure (TB) bronze was doped with nickel (Ni2+) with stoichiometry type $KSr_2Ni_xNb_{5-x}O_{15-\delta}$ onde x = 0,25; 0,50 and 0,75. The powders were prepared by chemical synthesis using the modified Polyol method, and characterized by infrared spectroscopy with Fourier transform (FT-IR), by X-ray diffraction (XRD), including the network parameters (relative intensity - $I_{R(KSNNi0,50)}$ **>** $I_{R(KSNNI0,25)}$ **>** $I_{R(KSNNI0,75)}$) and crystallite size. The effects of doping (Ni2+) in the process of photo degradation were studied, the absorbance as a function of time for the Basic Blue dye 41 result from the photo degradation performed with the photo catalyst KSNNi0,50 presented a lower absorbance value, and the spectrophotometer was used in the UV-vis region. The efficiency and kinetics of better photo catalytic degradation of Basic Blue 41 by catalysts $KSr_2Ni_xNb_{5-x}O_{15-\delta}$ where x = 0,25; 0,50 and 0,75 was the system $KSr_2Ni_xNb_{5-x}O_{15-\delta}$ where x = 0,50 which was discussed.

Keywords: *heterogeneous catalysis; oxidative catalysts; photo catalysts, niobate; tetragonal tungsten bronze structure; basic blue 41.*

GJRE-C Classification: *For Code: 290601*

Strictly as per the compliance and regulations of:

Chemistry Synthesis, Characterization and Photocatalysis of $KSr_2Nb_5O_{15}$ Doped with Nickel

Paulo César Faria

Abstract- Potassium and strontium niobate ($KSr_2Nb_5O_{15}$) of tungsten structure (TB) bronze was doped with nickel (Ni^{2+}) with stoichiometry type $KSr_2Ni_xNb_{5-x}O_{15-\delta}$ onde x = 0,25; 0,50 and 0,75. The powders were prepared by chemical synthesis using the modified Polyol method, and characterized by infrared spectroscopy with Fourier transform (FT-IR), by X-ray diffraction (XRD), including the network parameters (relative intensity - $I_{R(KSNNi0,50)} > I_{R(KSNNI0,25)} > I_{R(KSNNI0,75)}$) and crystallite size. The effects of doping (Ni^{2+}) in the process of photo degradation were studied, the absorbance as a function of time for the Basic Blue dye 41 result from the photo degradation performed with the photo catalyst $KSNNi_{0,50}$ presented a lower absorbance value, and the spectrophotometer was used in the UV-vis region. The efficiency and kinetics of better photo catalytic degradation of Basic Blue 41 by catalysts $KSr_2Ni_xNb_{5-x}O_{15-\delta}$ where x = 0,25; 0,50 and 0,75 was the system $KSr_2Ni_xNb_{5-x}O_{15-\delta}$ where x = 0,50 which was discussed.

Keywords: heterogeneous catalysis; oxidative catalysts; photo catalysts, niobate; tetragonal tungsten bronze structure; basic blue 41.

I. Introduction

The chemical contamination of the water covers a large spectrum of pollutants. The textile and leather industries are mainly responsible for the discharge of these large quantities of dyes. The highly colored effluents from these industries are affecting the nature of water, inhibiting the penetration of sunlight and reducing photosynthetic reactions, ATAR et al. (2008)[1]. Approximately 10-15% of these dyes are not fixed to the substrates during the dyeing process, as some dyes used in the textile industry and their biodegradation by-products may have a high degree of toxicity, mutageni city and carcinogenicity to humans; FRAGAA, ZANONIA (2009)[2]. These Dye effluents are difficult to treat by conventional methods and cannot be completely degraded. Heterogeneous photo catalysis has aroused great interest, with the aim of efficiently purifying waste water containing dyes; ZHANG et al (2009)[3].

Basic Blue 41 dye boasts an azo chromophore group and is used in the dyeing of synthetic fibers such as polyamide, polyester and viscose. Basic (cationic) dyes, which mostly have hydrolysis stability, are pH sensitive and are soluble in aqueous medium. Therefore, they require more efficient treatment methods for their complete removal in surface waters and effluents; FRAGAA, ZANONIA (2009)[2].

The photo catalytic reactions on semiconductor surfaces are processed according to the basic steps of: excitation with light of energy greater than the band gap (Eg), of the semiconductor, generation of electron/gap pairs (e-/h+); imprisoning electrons and gaps by adsorbed species. The mechanism of redox processes mediated by semiconductors in aqueous media promotes the formation of the hydroxyl radical (OH•), powerful oxidizing agent, generated by promoting the oxidation of the water / hydroxyl adsorbed by the lacuna, making the photo catalytic process highly efficient to oxidize most of the organic compounds. The efficiency of this process is related to the lifetime of the gaps (h+bv) and retardation of the recombination velocity of the generated loads (e-/h+) in the semiconductor; FRAGAA, ZANONIA (2009)[2].

Although titanium dioxide is currently the most widely used, niobate based photo catalysts have been extensively studied because of their excellent photo catalytic properties, such as KNb_3O_8, $K_6Nb_{10.8}O_{30}$, $K_4Ce_2M_{10}O_{30}$ (M=Ta, Nb), NiM_2O_6 (M=Nb, Ta), $K_4Nb_6O_{17}$, $BiNbO_4$, NiO-$KTiNbO_5$, etc. Among these niobate photo catalysts, $K_4Ce_2M_{10}O_{30}$ (M=Ta, Nb), NiM_2O_6 (M=Nb , Ta), NiO-$KTiNbO_5$ e $K_4Nb_6O_{17}$ high photo catalytic activity was found in the field of water decomposition. The KNb_3O_8, $K_6Nb_{10.8}O_{30}$ and $BiNbO_4$ were studied for the degradation of dyes. However, the potassium and strontium type niobates (TTB) $KSr_2Nb_5O_{15}$ showed high photo catalytic activity in the degradation of red acid G under irradiation UV degrading and breaking the nitrogen double bond (−N=N−), and also causes the double bonds of the benzene and naphthalene rings to split up, the degradation rate exceeds 85% and its kinetics remains the first order; ZHANG et al. (2009)[3].

Recent studies of the $KSr_2Nb_5O_{15}$ attests its photo catalytic activity resulting in methy lene blue photo oxidation as a model reaction. These niobates $KSr_2Nb_5O_{15}$ present higher catalytic activity with lower calcination time, and under very low concentration conditions under irradiation UV; MATOS et al. (2017)[4].

The present work aims to analyze the photo catalytic potential of materials with stoichiometry $KSr_2(Ni_xNb_{5-x})O_{15-\delta}$, where its substitutions with nickel metal vary $0,25 \leq x \leq 0.75$, $K\,Sr_2\,(Ni_{0,25}Nb_{4,75})\,O_{15\,-\delta-}$

Author: Science and Technology School – University of the State of São Paulo "Júlio de Mesquita Filho" CEP. e-mail: lacfaria@gmail.com

($KSNNi_{0,25}$); $KSr_2(Ni_{0,50}Nb_{4,50})O_{15-\delta}$ - ($KSNNi_{0,50}$) and $KSr_2(Ni_{0,75}Nb_{4,25})O_{15-\delta}$ - ($KSNNI_{0,75}$) calcined 1250°C/1h.

II. Experimental Procedures and Characterizations

a) Synthesis

The Modified Polyol Method LI et al. (2006)[5], FELDMAN (2005)[6], Vivekananghan, Venkateswarlu, Satyanarayana (2004)[7], Xu, Huang, Long (2003)[8], Sun Et Al. (2002)[9][5-9], was used for the chemical synthesis of the following systems $KSr_2(Ni_xNb_{5-x})O_{15-\delta}$ (where $0,25 \leq x \leq 0.75$), $KSr_2Ni_{0,25}Nb_{4,75}O_{15-\delta}$; $KSr_2Ni_{0,5}Nb_{4,5}O_{15-\delta}$ e $KSr_2Ni_{0,75}Nb_{4,25}O_{15-\delta}$ Lanfredi Et Al. (2012)[10]; Dantas, Lanfredi, Nobre (2012)[11] E Gutiérrez, Saldivar, Lopez (2008)[12][10-12]. This method allows better control of reagents, low calcination temperatures, single-phase materials and high surface area dust, Lanfredi et al. (2014)[13]; Hsiao et al. (2012)[14]; LANFREDI et al. (2011)[15] e Nobre, Lanfredi (2003)[16][13-16].

The starting reagents for the synthesis by chemical method were nitric acid, HNO_3(65,5% Reagen), strontium carbonate, $SrCO_3$ (99,0% Reagen), Potassium carbonate, K_2CO_3 (99,0% Reagen), ethylene glycol, $HOCH_2CH_2OH$ (98,0% Synth), nickel oxide, Ni_2O_3 (99,5% Reagen) and the ammoniacal oxalate salt of niobium, NH_4H_2 $[NbO(C_2O_4)_3]$ $.3H_2O$ (CBMM-Brasil).

The precursor reagents for the preparation of the solution were dissolved in nitric acid with continuous stirring in the beaker. Then, 100 ml of ethylene glycol was added. The solution was heated to 90 ° C, promoting the decomposition of the NO_3 group, similar to the process developed in the Pechini method, NOBRE (1995)[17]; NOBRE (1999)[18]; PECHINI (1967)[19] e LANFREDI et al. (2014)[20][17-20]. After complete evaporation of the gas it was observed the formation of a polymeric gel (polyesterification reaction), where it was subjected to a pre-calcination. This polymer is maintained in the beaker to undergo a primary calcination in a box type furnace. This pre-calcination was performed in two stages. In the first step, from room temperature, the temperature was increased at a rate of 10 °C/min until it reaches the temperature of 150 °C, which was held constant for 1 hour for the elimination of low molecular mass molecules, as water molecules. Following, maintaining the same heating rate, the temperature was raised to 300 °C, being maintained at that temperature for 2 hours. This pre-calcination was carried out under a N_2(g) with flow of 500 mL/min. The cooling was carried out at the natural rate of the furnace, maintaining the nitrogen flow.

The process results in partial decomposition of the polymer to form a resin, which consists of a brittle reticulated material. This material was deag glomerated in agate-mortar and sieved in mesh 350 meshes with opening of 45 μm, being called precursor powder. Afterwards the steps of deag glomeration and sifting exhibiting fine and homogeneous show. Calcination was carried out at 1250 °C during 1 h, heating rate of 10 °C/min.

b) Characterization Techniques

The post-ceramics based on strontium and potassium niobate ($KSr_2Nb_5O_{15}$) with stoichio metry $KSr_2Ni_{0,25}Nb_{4,75}O_{15-\delta}$; $KSr_2Ni_{0,50}Nb_{4,5}O_{15-\delta}$ and $KSr_2Ni_{0,75}Nb_{4,25}O_{15-\delta}$ were characterized by absorption spectroscopy in the infrared region (FT-IR), X-ray diffraction (DRX) then its photo catalytic potential was evaluated.

i. *Microscopia Eletrônica de Varredura (MEV)*

ii. *Infrared with Fourier Transform (FT-IR)*

The infrared spectral absorption spectroscopy was performed in a spectrophotometer of the brand SHIMADZU model IRAffinity-1. The spectral range used was in the medium infrared region (3500 – 450 cm^{-1}), with resolution of 8 cm^{-1} and 120 scans. The samples were dispersed in KBr in the proportion of 1:100. Potassium Bromide tablets (KBr) were prepared using a tablet of the mark PIKE de 13 mm diameters in hydraulic press of 10 ton. Each tablet was produced by macerating 1,5 mg of the sample, ceramic powders, with 0,30 g de KBr in agate mortar. The mixture with KBr was pressed in the pellets by 10 min. The tablet thus obtained was analyzed in a spectrophotometer.

iii. *X-ray diffractometry (XRD)*

The precursor post-ceramics, the solid solutions of $KSr_2(Ni_xNb_{5-x})O_{15-\delta}$, where the x = 0,250; 0,500 e 0,750 producing stoichio metrically the following materials: $KSr_2Ni_{0,25}Nb_{4,75}O_{15-\delta}$, $KSr_2Ni_{0,50}Nb_{4,5}O_{15-\delta}$ and $KSr_2Ni_{0,75}Nb_{4,25}O_{15-\delta}$ and treated at temperatures of 1250°C, were characterized by X-ray diffraction using a diffracto meter SHIMADZU (model XRD-6000), with radiation Cu K α (λ=1,54060 Å), operating at 40kV and 30mA, in the range of $5 \leq 2\theta \leq 80$, with scan time of 1,00°/min, steps of 0,02° and time per step equal to 1,20s. The slits of divergence and scattering used were 1,00° and the receiving slot of 0,30 mm.

a. *Network Parameters*

The network parameters are calculated using the "Least Squares". The positions $2\boldsymbol{\theta}_0$, the plans hkl, the type of the crystalline structure, the number of interactions to be executed, are the program data.

b. *Average crystallite size*

The values of the mean crystallite size for the solid solutions of $KSr_2(Ni_xNb_{5-x})O_{15-\delta}$, where a) x = 0,25; b) x = 0,50 and c) x = 0,75 were calculated by the Scherrer equation, equation (1).

$$D = \frac{K\lambda}{\beta \cos\theta} \quad (1)$$

being β the width of the peak where the intensity is half of its maximum value denominated (peak width at half height), θ is the angle corresponding to the diffraction, λ is the wavelength of the Cu (1,5406 Å), k is the constant of proportionality, called the particle shape factor (TB = 0,89) NUFFIELD (1986)[21].

c) Evaluation of photo catalytic potential

For the study of photo catalytic activities, we used the degradation material Basic Blue 41 in aqueous solutions. The photo catalytic tests will be performed in order to maximize the activation of the post-ceramics as a catalyst.

d) Photo catalytic procedure of Basic Blue 41 dye

To investigate the photo catalytic activity of the ceramic powders, a photo catalytic reactor. This low power photo catalytic reactor has a source of irradiation, a light bulb with dimensions (length 438,0 mm, diameter 26,0 mm) HSN® 15 W G13 which emits radiation at the wavelengths UVC between 200 to 280 nm, that is, specifically 250 nm, which corresponds to the range of the electromagnetic spectrum of ultraviolet C (rays UV-C). In this way the photo catalytic activity of the material was studied using as comparative parameter tests with UV-C. For the light bulb the measured irradiance was 0,3 mW/com^2 during the photo catalytic test stage and the measured irradiance of 1,8 mW/cm^2.

Basic blue 41 solutions were prepared by means of a dilution of the stock solution, thus obtaining a concentration of 40 ppm. The pH of the solution was then measured through a pH meter (GEHAKA) adjusting the pH to 8 in some tests with the aid of a few drops of sodium hydroxide 0,01mol.L^{-1} and in other tests the natural pH of the solution was maintained for the purpose of comparison with the original methodology using the ceramic powders. Was heavy 0,125g of catalyst, in order to obtain optimum concentration of catalyst (0,55 g.L^{-1}) in a volume of 1000 mL of solution (12,5 mg/L).

The first step consists of the photo catalytic tests of a period of 1 hour, where at the beginning of the first 60 minutes the post-ceramics were added in solution of Basic Blue 41, with the flow of water circulating through the reactor, with the help of a small compressor, in order to reach the equilibrium of adsorption-desorption in the dark, this is the step in the dark, process of accommodation of the material to solution. The last 30 minutes with the reactor lamp on and continuous flow. In the last minutes (photolysis) at 59 minutes, a 5.0 mL aliquot of the sample was collected by means of a volumetric pipette, starting the removal of the first sample, identified (t = 0).

The second step of the photo catalytic tests were the collections every 15 minutes totaling 1 h, and identified= 1, 2, 3 e 4.

The third step of the photo catalytic tests, the collections were performed every 30 minutes, totaling 2 h and identified by t= 5, 6, 7, 8, 9 e 10, totaling 11 samples collected.

In the fourth step, the collected samples were accommodated in test tubes enclosed in boxes avoiding exposure to light. These test tubes were centrifuged, 3000 rpm by 20 minutes, in order to separate the catalyst from the solution, 0,5 mL of the sample (supernatant) with the aid of a Pasteur pipette, and diluted 5 mL of distilled and deionized water, measured with a volumetric.

In the fifth step, the supernatants were analyzed in a UV-vis spectrophotometer and programmed for wavelength reading (λ) 611 nm of the solution, recording the absorbance of the samples.

e) Determinação da Eficiência e Parâmetro Cinético de Degradação

The photo catalytic activity of post-ceramics $KSr_2(Ni_xNb_{5-x})O_{15-\delta}$, where x= 0,25; 0,50 and 0,75 the kinetics of the disappearance of Basic Blue 41 as test molecule.

In order to establish the photo catalytic behavior of niobate based materials, both degradation kinetics and direct photolysis in the absence of solids were followed. The disappearance of the Basic Blue dye 41 was reported in terms of the conversion (X) obtained by the following expression of the efficiency represented by the concentration equation (2):

$$X = \left[\left(\frac{C_o - C_t}{C_o}\right)\right].100 \cong \left[\frac{(A_0 - A_t)}{A_0}\right].100 \quad (2)$$

Where Co is the initial concentration of Basic Blue dye 41, Ct is the concentration in reaction time t, and ao and at are the initial absorbance and the absorbance at the reaction time t. In this way he analyzed and studied the efficiency and kinetics of degradation of the dye Basic Blue 41.

III. Results and Discussions

a) Infrared with Fourier Transform (FT-IR)

Figure 1 (a, b e c) - ($KSNNi_{0,25}$; $KSNNi_{0,50}$ and $KSNNi_{0,75}$) shows the infrared (IR) vibration absorption spectra for the stoichio metric systems $KSr_2(Ni_xNb_{5-x})O_{15-\delta}$ onde a) x = 0,25; b) x = 0,50 and c) x = 0,75. These spectra present bands in the range of 450 to 1100 cm^{-1}, such bands are characteristic of the connections Nb-O for regions of low frequencies, attributed to the antisym metrical stretching for the connection ν_{as} (Nb-O), symmetrical stretching ν_s (Nb-O-Nb), symmetrical stretching ν_s (Nb-Oap). The displacements in the spectra show that the bonds between niobium and oxygen cations are shorter in relation to host structure ($KSr_2Nb_5O_{15}$) DENIO et al. (2010)[22]; YEBIN, GUOHUA, HUA (2003)[23] and

BERGAMASCHI (2000)[24][22-24], this system has characteristic bands that identify the presence of an "envelope" and with the addition of nickel (Ni-O) to $KSr_2Nb_5O_{15}$; YEBIN, GUOHUA, HUA (2003)[23] tends to displace the system bands. Symmetrical stretching is attributed (ν_s) and antisym metric (ν_{as}) DENIO et al. (2010)[22] and BERGAMASCHI (2000)[24].

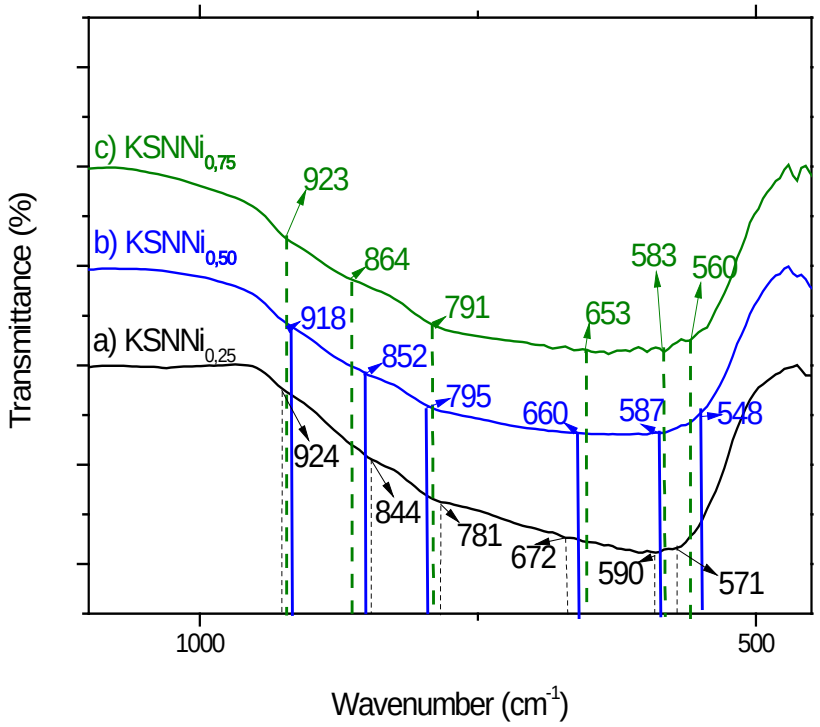

Fig. 1: Vibrational spectrum in the region of 450-1100 cm^{-1} of infrared, for stoichio metric systems $KSr_2(Ni_xNb_{5-x})O_{15-\delta}$ where a) x = 0,25; b) x = 0,50 and c) x = 0,75 denominated $KSNNi_{0,25}$, $KSNNi_{0,50}$ and $KSNNi_{0,75}$.

Figure 1 (a) - ($KSNNi_{0,25}$) shows a portion of the spectrum in the infrared region where it is characterized by an envelope in the region between 450 – 1100 cm^{-1} for the system $KSr_2(Ni_xNb_{5-x})O_{15-\delta}$ where a) x = 0,25. In this figure, the spectra show bands of strong intensity below 1000 cm^{-1}, characteristic of niobatos. The bands identified have wavelengths in 571, 590, 672, 781, 844 and 924 cm^{-1} such band refer to the oxide-metal bonds.

Figure 1 (b) - ($KSNNi_{0,50}$) shows parts of the spectrum in the infrared region where it is characterized by an envelope in the region between 450 – 1100 cm^{-1} for the system $KSr_2(Ni_xNb_{5-x})O_{15-\delta}$ where b) x = 0,50. In this figure, the spectra show bands of moderate intensity below 1000 cm^{-1}, characteristic of niobatos. The bands identified have wavelengths in 548, 587, 660, 795, 852 and 918 cm^{-1} such band are attributed to the oxide-metal bonds.

Figure 1 (c) - ($KSNNi_{0,75}$) shows parts of the spectrum in the infrared region where it is characterized by an envelope in the region between 450 – 1100 cm^{-1} for the system $KSr_2(Ni_xNb_{5-x})O_{15-\delta}$ where c) x = 0,75. In this figure, the spectra show bands of moderate intensity below 1000 cm^{-1}, characteristic of niobatos. The bands identified have wavelengths in 560, 583, 653, 791, 864 and 923 cm^{-1} such band are attributed to the oxide-metal bonds. Table 1 below shows the low intensity and high intensity wave numbers for stoichio metric systems $KSr_2(Ni_xNb_{5-x})O_{15-\delta}$ where x = 0,25; 0,50 and 0,75.

Table 1: Absorption band positions, associated with each stoichio metry of the $KSr_2(Ni_xNb_{5-x})O_{15-\delta}$ where x = 0; 0,25; 0,50 and 0,75.

Stoichiometric system	Wavenumber (cm^{-1})					
$KSr_2(Ni_{0,25}Nb_{4,75})O_{15-\delta}$	571	590	672	781	844	924
$KSr_2(Ni_{0,50}Nb_{4,50})O_{15-\delta}$	548	587	660	795	852	918
$KSr_2(Ni_{0,75}Nb_{4,25})O_{15-\delta}$	560	583	653	791	864	923

From the data in Table 1 it was observed a displacement of the bands characteristic of the connections Nb-O and Nb-O-Nb for regions of low frequencies with increasing concentration of nickel cations. The narrower and lower intensity bands move to regions with higher wave numbers, around 571 to 590 cm^{-1} to $KSr_2(Ni_{0,25}Nb_{4,75})O_{15-\delta}$; 548 to 587 cm^{-1} to $KSr_2(Ni_{0,50}Nb_{4,50})O_{15-\delta}$ and 560 to 583 to $KSr_2(Ni_{0,75}Nb_{4,25})O_{15-\delta}$. These bands are attributed to stretching (Nb-O). The medium and wide asymmetric bands in the regions of 672 cm^{-1} to 781 cm^{-1}, observed in the spectrum of $KSr_2(Ni_{0,25}Nb_{4,75})O_{15-\delta}$ they move to regions between 660 cm^{-1} to 795 cm^{-1} spectra of the solid solutions of $KSr_2(Ni_{0,50}Nb_{4,50})O_{15-\delta}$ and this system for 653 cm^{-1} to 791 cm^{-1} for the system $KSr_2(Ni_{0,75}Nb_{4,25})O_{15-\delta}$. The bands in the region between 844 cm^{-1} to 924 cm^{-1} can be attributed to the symmetrical (Nb-O-Nb) LANFREDI, FOLGUERAS-DOMÍNGUES, RODRIGUES (1995)[25]. The displacement of these bands to the region of smaller wave number in the spectra of the solid solutions of the $KSr_2(Ni_{0,25}Nb_{4,75})O_{15-\delta}$, $KSr_2(Ni_{0,50}Nb_{4,50})O_{15-\delta}$ and $KSr_2(Ni_{0,75}Nb_{4,25})O_{15-\delta}$, shows that the bonds between niobium and oxygen cations are shorter.

b) X-ray diffractometry (XRD)

Figure 2 shows the X-ray diffracto grams obtained for the precursor powders of the stoichio metric system based on niobate KSr2(NixNb5-x)O15-δ where x= 0,25; 0,5 and 0,75 heat treated at 1250 ° C for 1 hour, in an oxygen atmosphere. X-ray diffracto grams show an increase in the definition of diffraction peaks to 1250°C, associated with the decrease of the microde formation of the net and increase of the structural stability. According, LANFREDI et al. (2005)[26], in solid solutions of $KSr_2(Ni_xNb_{5-x})O_{15-\delta}$ is adopted the valence of the Ni^{2+}, since the oxidation state +3 of nickel cation (Ni) has been rarely detected. The substitution of radium cations (r) such as the Sr^{2+} (rSr^{2+} = 1,18 Å) by cations of lightning (r) small, as the Ni^{2+} (rNi^{2+} = 0,69 Å) not favorable. In addition, the cations of Ni^{2+} show strong preference for octahedral coordination, the same coordination of niobium (Nb). In this sense, the ionic radius of Nb cations in a high oxidation state (rNb^{5+} = 0,64 Å), similarity with the ionic radius of the Ni^{2+}. However, the valence difference is equal to three units, which is not favorable. However, the best similarity of the ionic Ni^{2+} occurs for the Nb^{5+} partially reduced to Nb^{4+} (rNb^{4+} = 0,68 Å). Here it is important to comment that the Nb^{4+} represents a partial reduction of the niobium cation, whereas a completely reduced state is given by the niobium with valence 3+, Nb^{3+}, (rNb^{3+} = 0,72 Å).

The structural characterization of the post-ceramics constituted by the $KSr_2(Ni_xNb_{5-x})O_{15-\delta}$ where x= 0,25; 0,50 e 0,75 obtained by the modified Polyol chemical method was investigated and analyzed by means of the X-ray diffraction technique. The standard XRD for the system $KSr_2(Ni_xNb_{5-x})O_{15-\delta}$ with a range of 2θ of 5° - 80° is shown in Fig. 1 (0,25; 0,50 e 0,75). According to the crystal data file JCPDS 34-0108 (2000)[27], the system is of tetragonal type and presents spatial group P4bm (100). The diffracto grams of the samples that were prepared and calcined at 1250 ℃ / 1h fit the pattern, and in some angles (***θ***) present significantly lower displacements, which may consider that these samples consist of single phase for the compounds with variation of doping. The Diffracto gram shown in figure 2 (0,25) referring to the system $KSr_2(Nb_{5-x})O_{15-\delta}$ where x = 0,25 presents formation of a single crystalline phase based on the tetragonal symmetry of the crystallographic sheet JCPDS: 34-0108 (2000)[27] related to the niobium oxide strontium and potassium ($KSr_2Nb_5O_{15}$). as for the values of the müeller index (hkl), of 2***θ***, of ***θ***, of the interplanar distances (nm) and the intensities can be seen in table 1 below.

Figure 2 (0.50) shows the X-ray diffracto gram obtained by the system precursor powder $KSr_2(Ni_xNb_{5-x})O_{15-\delta}$ where x=0,50 a 1250 °C/1h calcined in an oxygen atmosphere. The diffracto gram, similar to figure 1 (0.25), shows crystalline phase formation indicated in the indexing of the crystallographic data sheet JCPDS: 34-0108 (2000)[27] tetragonal symmetry for this system $KSr_2Nb_5O_{15}$ the narrow peaks indicating an increase in the crystallinity of the calcined material are observed in this diffracto gram (Fig. 2 (0.25, 0.50 and 0.75)) the 1250 °C / 1h.

Figure 2 (0.75) shows the X-ray diffracto gram obtained by the $KSr_2(Ni_xNb_{5-x})O_{15-\delta}$ where x=0,75 calcined 1250 ° C / 1h and obtained in an oxygen atmosphere. This characterization showed the formation of the monophasic and crystalline powder ($KSNNi_{0,75}$). According to the data of this record, the phases found have a tetragonal structure compatible with the spatial group P4bm (100).

i. *Network Parameters*

The values given in tables 2 and 3 refer to the crystallographic sheet JCPDS: 34-0108 (2000)[27] shows the network parameters used to obtain the results of the interplanar distances and the ***θ***.

Table 2: Values of müeller index (hkl), of 2θ, of θ, of interplanar distances (nm) and the intensities, acquired in the crystallographic sheet JCPDS: 34-0108 (2000)[27] for the system $KSr_2Nb_5O_{15}$.

Hkl	2θ	θ	$d_{interplanar}$ (nm)	Intensidade
(400)	28.626	14.313	3.1	12
(311)	32.076	16.038	2.8	100
(002)	46.013	23.01	1.9	36
(422)	57.205	28.6025	1.6	31
(731)	61.297	30.65	1.5	6
(622)	67.112	33.56	1.4	7

However, the results data referring to table 3 refers to stoichio metric systems $KSr_2(Ni_{0,25}Nb_{4,75})O_{15-\delta}$. $KSr_2(Ni_{0,50}Nb_{4,50})O_{15-\delta}$. $KSr_2(Ni_{0,75}Nb_{4,25})O_{15-\delta}$ doped with nickel, where x = 0,25; 0,50 e 0,75.

Table 3: Values of the müeller index (hkl), of 2θ, of θ, of interplanar distances (nm) and the intensities for stoichio metric systems $KSr_2(Ni_{0,25}Nb_{4,75})O_{15-\delta}$. $KSr_2(Ni_{0,50}Nb_{4,50})O_{15-\delta}$. $KSr_2(Ni_{0,75}Nb_{4,25})O_{15-\delta}$.

Hkl	2θ	θ	$d_{interplanar}$ (nm)	Intensidade
$KSr_2(Ni_{0,25}Nb_{4,75})O_{15-\delta}$	27,9	13,95	3,2	1.003,5
	29.7	14,85	3,0	1.300,3
	32,3	16,15	2,8	2.308,9
$KSr_2(Ni_{0,50}Nb_{4,50})O_{15-\delta}$	27,9	13,95	3,2	2.449,4
	29,7	14,85	3,0	3.047,3
	32,2	16,1	2,7	5.104,6
$KSr_2(Ni_{0,75}Nb_{4,25})O_{15-\delta}$	27,9	13,95	3,2	1.631,8
	29,8	14,9	2,9	1.865,1
	32,2	16,1	2,7	3.455,5

The relative intensity (IR) for stoichio metric systems $KSr_2(Ni_{0,25}Nb_{4,75})O_{15-\delta}$, $KSr_2(Ni_{0,50}Nb_{4,50})O_{15-\delta}$ e $KSr_2(Ni_{0,75}Nb_{4,25})O_{15-\delta}$ follows the descending order.

$I_{R(KSNNi\mathbf{0,50})} > I_{R(KSNNI\mathbf{0,25})} > I_{R(KSNNI\mathbf{0,75})}$

ii. *Crystallite size*

The crystallite size of the solid solutions $KSr_2(Ni_xNb_{5-x})O_{15-\delta}$ where x = 0,25; 0,5 and 0,75 was determined using the program Jade 8 Plus. The widening of the mean width at half height (FWHM) of the diffraction peaks of the experimental diffracto gram was considered. The Jade 8 Plus program calculates the mean crystallite size by applying the Scherrer equation; AZÁROFF, BUERGUER (1958)[28]. Where D is the average crystallite size, *k* is the proportionality constant, which depends on the shape of the particles (TB = 0,89)^2, λ is the wavelength of the Cu (1,5406 Å), β is the width at half height of the corrected peak and θ the angle corresponding to the diffraction. The instrumental factors were corrected using the Silicon (Si) standard. The crystallite size KSN pure and doped with Nickel Method Modified polyol calcined for 1 hour, follows table 4.

Table 4: Mean crystallite size for solid solutions of stoichiometric systems $KSr_2(Ni_{0,25}Nb_{4,75})O_{15-\delta}$; $KSr_2(Ni_{0,50}Nb_{4,50})O_{15-\delta}$ $KSr_2(Ni_{0,75}Nb_{4,25})O_{15-\delta}$ doped with nickel where x = 0,25; 0,50 e 0,75 and calculated by the Scherrer equation.

Stoichiometric system	Crystallite size - calcination at 1250 °C / 1h
$KSr_2(Ni_{0,25}Nb_{4,75})O_{15-\delta}$	20,85 nm
$KSr_2(Ni_{0,50}Nb_{4,50})O_{15-\delta}$	23,70 nm
$KSr_2(Ni_{0,75}Nb_{4,25})O_{15-\delta}$	27,00 nm

The largest crystallite size was observed for solid solution $KSr_2(Ni_{0,75}Nb_{0,25})O_{15-\delta}$. The increase in the mean crystallite size with increasing the value of x to 0.75 is related to a greater distortion of the unit cell, increasing the diffusion process and nucleation of the crystals; MELO (2007)[29]. These values show that the increased dopant concentration promotes an increase in structural anisotropy in the material; DANTAS et al. (2009)[30]. According to the values in Table 4, the value of the average size of network crystallite increases as the x value increases from 0.25 to 0.75. This effect is a consequence of the high degree of doping of the host structure, where an excess of nickel cations causes a disorder in the crystalline lattice to form defects, caused by non-stoichio metry of the structure; WANG et al. (2012)[31].

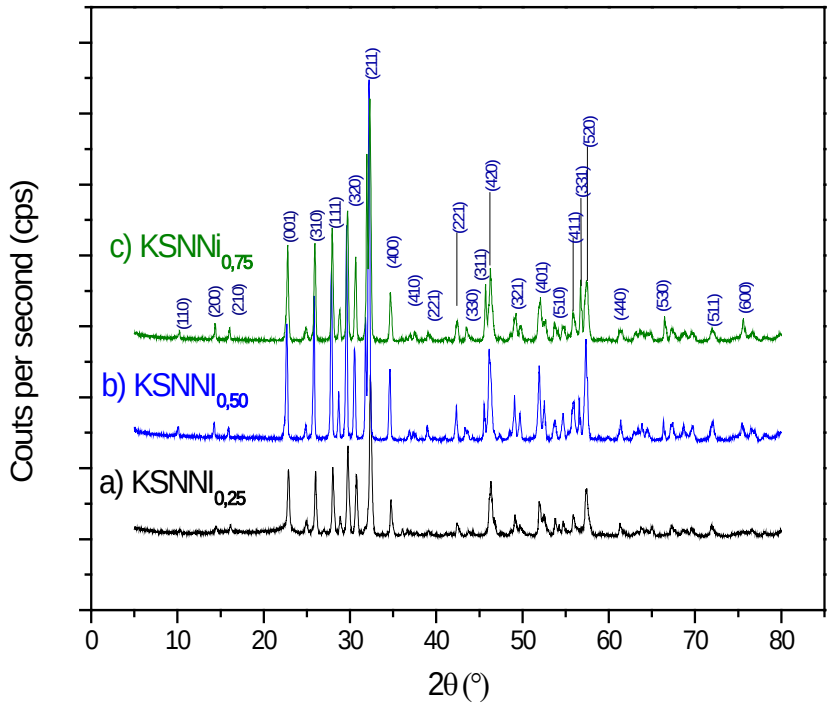

Fig. 2: Difratograma de raios X dos sistemas estequiométricos $KSr_2(Ni_{0,25}Nb_{4,75})O_{15-\delta}$ – ($KSNNi_{0,25}$), do $KSr_2(Ni_{0,50}Nb_{4,50})O_{15-\delta}$ – ($KSNNi_{0,50}$) e do $KSr_2(Ni_{0,75}Nb_{4,25})O_{15-\delta}$ – ($KSNNi_{-0,75}$) calcinados a 1250 °C / 1h em atmosfera de oxigênio.

In this diffracto gram between 20 and 35 displayed on the 2$\boldsymbol{\theta}$ scale there is a close junction between peaks in relation to figure 2, the crystal plug, JCPDS: 34-0108 (2000)[27] follows partially offset from the peaks. The values of the interplanar distances, the relative intensity and the 2$\boldsymbol{\theta}$ of the diffracto gram coincide with the values listed on this sheet. The lines of this chart coincide with the diffracto gram peaks, however, it is possible to notice a singular difference between these peaks, as regards the relative intensity with the lowest intensity (Figure 2 - c) $KSNNi_{0,75}$) in relation to the relative intensity of b) $KSNNi_{0,50}$ in Figure 2, where in this diffracto gram the intensity of the peaks is much more expressive and defined, but of a considerable narrow width.

c) *Avaliação do potencial fotocatalítico: Determinação da eficiência e Cinética de degradação*

Figure 3 - a) $KSNNi_{0,25}$; b) $KSNNi_{0,50}$ and c) $KSNNi_{0,75}$ shows the absorbance as a function of time, the adsorption in the dark for 1h and the degradation rate with the reactor connected for 3h together with the photo degradation kinetics with irradiation of UV light. Figure 4 shows the rate of discoloration over time for a) $KSNNi_{0,25}$; b) $KSNNi_{0,50}$ and c) $KSNNi0_{,75}$ and Fig. 5 shows the Ln (C_0/C_t) depending on the time for the systems (a) $KSNNi_{0,25}$; b) $KSNNi_{0,50}$ and c) $KSNNi0_{,75}$ to investigate the degradation of Basic Blue 41. The performance of the materials synthesized here can be observed that the rate of adsorption is very fast for all catalysts, reaching the equilibrium of the dye after 30-60 min. Thus, photocatalytic tests with UV light irradiation were performed after an initial 60 min adsorption period. It is interesting to note that the amount of Basic Blue 41 adsorbed has decreased over time.

d) *Efficiency and rate of degradation of $KSNNi_{0,25}$; $KSNNi_{0,50}$ and $KSNNi_{0,75}$*

The first test was performed with the stoichio metry material $KSr_2(Ni_xNb_{5-x})O_{15-\delta}$ where x = 0,25 irradiated with UV light and catalyst 0,10g and concentration of 12,5 $mg.L^{-1}$ of the type dye (Basic Blue 41). Figure 3 shows the absorbance versus time of Basic Blue 41 using the material $KSNNi_{0,25}$. The moment the material is added $KSNNi_{0,25}$ the elapsed time solution of 1 h without UV irradiation at a drop in absorbance of 2.35%, This percentage is due to the fact of an accommodation of the solution to the surface of the catalyst, being that at the moment of the adsorption there was no degradation of the solution of Basic Blue 41. However, for the same material $KSNNi_{0,25}$ considering the last three hours the rate of discoloration was 91,35 % considering its absorbance, which leads us to believe that the degradation of Basic Blue 41 can be attributed to the photo catalytic effect of $KSr_2(Ni_xNb_{5-x})O_{15-\delta}$ where x = 0,25 under irradiation UV.

The second test performed with stoichiometry material $KSr_2(Ni_xNb_{5-x})O_{15-\delta}$ where x = 0,50 irradiated with UV light and catalyst 0,10g and concentration of 12,5 $mg.L^{-1}$ of the dye (Basic Blue 41). Figure 3 shows the absorbance versus time of Basic Blue 41 using the material Figure 3 shows the absorbance versus time of Basic Blue 41 using the material $KSNNi_{0,50}$. The moment the material is added $KSNNi_{0,50}$ the elapsed time of 1 h, without UV irradiation at a drop in absorbance of 4,00 %. This percentage is due to the fact that a solution solution to the surface of the catalyst, indicating a larger surface, and that at the moment of adsorption there was no degradation of the solution of Basic Blue 41. However, for the same material $KSNNi_{0,50}$ considering the last three hours the rate of discoloration was 97,51 % considering its absorbance, which leads us to believe that the degradation of Basic Blue 41 can be attributed to the photo catalytic effect of $KSr_2(Ni_xNb_{5-x})O_{15-\delta}$ where x = 0,50 under irradiation UV.

The third test performed with the stoichiometry material $KSr_2(Ni_xNb_{5-x})O_{15-\delta}$ where x = 0,75 irradiated with UV light and catalyst 0,10g and concentration of 12,5 $mg.L^{-1}$ of the dye (Basic Blue 41). Figure 3 shows the absorbance versus time of Basic Blue 41 using the material $KSNNi_{0,75}$. The moment the material is added $KSNNi_{0,75}$ the elapsed time of 1 h, without UV irradiation at a drop in absorbance of 3,00 %, This percentage is due to the fact that a solution to the surface of the catalyst, indicating a larger surface, and that at the moment of adsorption there was no degradation of the solution of Basic Blue 41. However, for the same material $KSNNi_{0,75}$ considering the last three hours the rate of discoloration was 97,51 % considering its absorbance, which leads us to believe that the degradation of Basic Blue 41 can be attributed to the photo catalytic $KSr_2(Ni_xNb_{5-x})O_{15-\delta}$ where x = 0,75 under irradiation UV.

It is important to emphasize that the adsorbed samples presented expected results due to the chemical nature of Basic Blue 41, this dye being a strong Lewis base, and its adsorption is thermodynamically favored by Lewis acidic solids, such as the materials synthesized here. According to surveys; MATOS et al. (2017)[4], in fact, these materials that are Lewis acids constituted of niobatos present high electronic affinity of their ions Nb (86,1 kJ / mol). This condition induces the agreement that niobate based catalysts have a more acidic surface pH and therefore have a high affinity for basic amines such as Basic Blue 41 with a high dissociation constant (pKb) and a high neutralization potential.

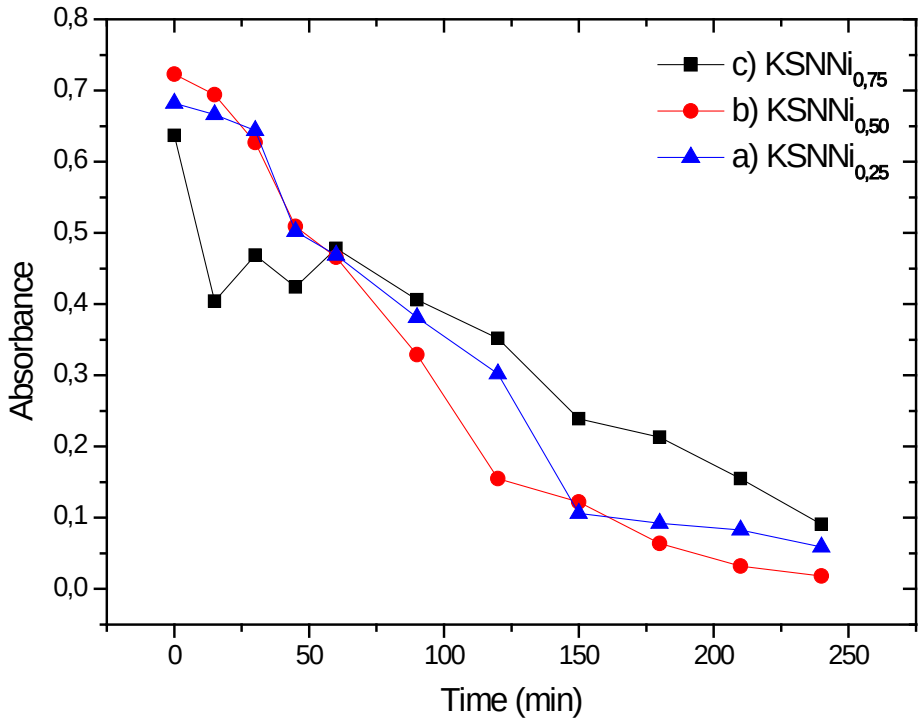

Fig. 3: Absorbance as a function of the degradation time of the Basic Blue 41 using the materials a) $KSNNi_{0,25}$; b) $KSNNi_{0,50}$ and c) $KSNNi_{0,75}$.

Absorbance readings at the maximum absorption wavelength of the "basic blue 41" dye were performed for the photo catalytic tests with the photo catalysts $KSNNi_{0,75}$; $KSNNi_{0,50}$ and $KSNNi_{0,25}$. According to figure 3 - a) $KSNNi_{0,25}$; b) $KSNNi_{0,50}$ and c) $KSNNi0_{,75}$ a decrease in the absorbance values versus time for all tests was observed indicating a decrease in the concentration of the basic blue 41 dye in solution resulting from the photo degradation. Among the photo catalytic tests performed, the photo catalyst test $KSNNi_{0,50}$ presented lower absorbance value.

From Figure 4 - a) $KSNNi_{0,25}$; b) $KSNNi_{0,50}$ and c) $KSNNi0_{,75}$ an increase in the rate of decolorization as a function of time is observed for all the photo catalytic tests performed, indicating a decrease in the concentration of the dye "basic blue 41". The photo catalyst that presented the highest discoloration rate was the $KSNNi_{0,50}$ so it was the most efficient.

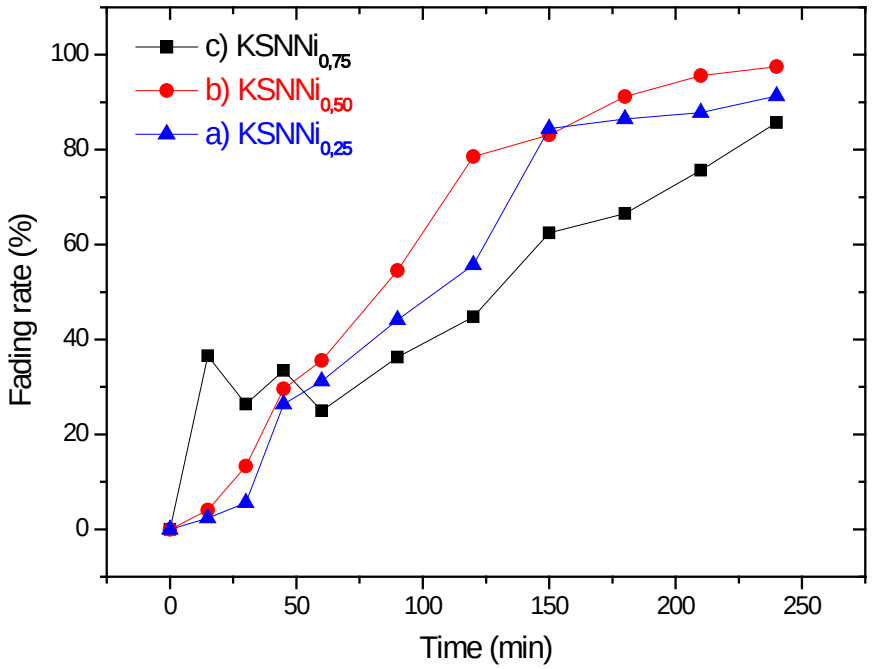

Fig. 4: Discoloration rate versus time for systems a) $KSNNi_{0,25}$; b) $KSNNi_{0,50}$ and c) $KSNNi_{0,75}$.

e) Kinetics of degradation of materials $KSNNi_{0,25}$; $KSNNi_{0,50}$ and $KSNNi_{0,75}$

Figure 5 - a) $KSNNi_{0,25}$; b) $KSNNi_{0,50}$ and c) $KSNNi_{0,75}$ shows the linear relationship ln (C_0 / Ct) as a function of the photo degradation reaction time t which indicates that the photo degradation reaction of the catalysts continues to be first order kinetics. For the catalyst $KSr_2(Ni_{0,25}Nb_{4,75})O_{15-\delta}$ which shows the linear relationship ln (C_0 / Ct) and photo degradation reaction time t indicates that the reaction continues being kinetic of first, according to kinetic equation. For Fig. 5 - b) $KSNNi_{0,50}$ shows the linear relationship ln (C_0 / Ct) and photo degradation reaction time t indicates that the photo degradation reaction of the catalyst $KSr_2(Ni_{0,50}Nb_{4,50})O_{15-\delta}$ also follows kinetics of first order, according to kinetic equation. For fig.5 - c) $KSNNi_{0,75}$ shows the linear relationship ln (C_0 / Ct) and photo degradation reaction time t indicates that the photo degradation reaction of the catalyst $KSr_2(Ni_{0,75}Nb_{4,25})O_{15-\delta}$ also follows first-order kinetics, according to kinetic equations.

On the other hand, the Figure 3 - a) $KSNNi_{0,25}$; b) $KSNNi_{0,50}$ and c) $KSNNi_{0,75}$ show very similar kinetic trends in the photo catalytic degradation of Basic Blue 41 for all photo catalysts $KSr_2(Ni_xNb_{5-x})O_{15-\delta}$ where x = 0,25; 0,5 and 0,75. To compare the photo activity, the first order apparent rate constants (k_{app}) were estimated from linear regression of kinetic data, and assuming that Basic Blue 41 photo degradation follows a first order reaction rate mechanism; FRAGAA, ZANONIA (2009)[2] e ATAR, OLGUN, ÇOLLAK (2008)[1] [1-2] . We attribute this photo activity due to the presence of apical oxygen atoms that are very reactive and are attached to the niobium in the octahedron [NbO_6] MATOS et al. (2017)[4].

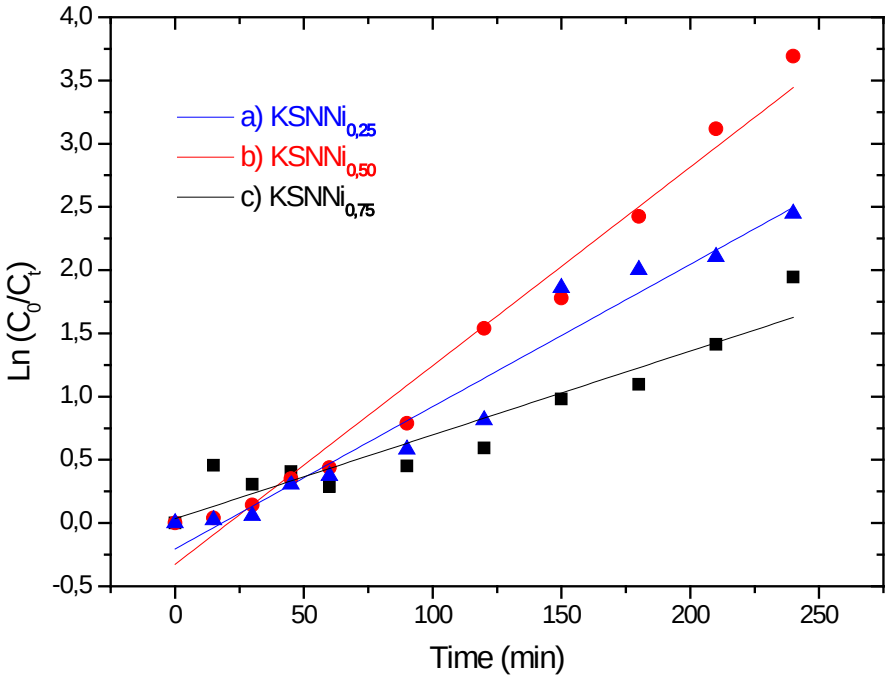

Fig. 5: Ln (C_0/C_t) depending on the time for the systems a) $KSNNi_{0,25}$; b) $KSNNi_{0,50}$ and c) $KSNNi_{0,75}$.

Analysis of the kinetic curves in all the photo catalytic tests performed shows a first order kinetics, the data shown in Table 1 confirm such observations.

Table 1: Summary of the kinetic parameters for the photocatalytic tests

Catalyzer	KSNNi0,25	KSNNi0,50	KSNNi0,75
K (min)	0,01125	0,01571	0,00663
$t_{1/2}$ (min)	61,61	44,12	104,55
R^2	0,95017	0,97412	0,88381
Kinetic Equation	$Ln(C_0/C_t) = -0,20445 + 0,01125$ x	$Ln(C_0/C_t) = - 0,32642 + 0,0151$ x	$Ln(C_0/C_t) = 0,03394 + 0,00663$ x

The photo catalytic test with the photo catalyst $KSNNi_{0,5}$ presented a higher speed constant and a shorter half-life, being the most efficient. According to the results, the nickel doping in the host structure of the $KSr_2Nb_5O_{15}$ promotes an increase of the photo catalytic activity until a substitution of 10% in mol of Ni^{2+}, and a decrease in photo catalytic activity can be observed for the KSN doped with 15 mol%.

IV. General Discussions

Solid state diffusion is a mass transport medium occurring within the solid materials according to an atomic movement occurring in stages. The mechanisms promoting this mass transport are realized by means of an exchange of atoms which is located in a normal position of the network with an adjacent gap or by a migration from an interstitial position to an adjacent empty interstitial position in which the host metal, the interstitial atomic species diffuse more rapidly, CALLISTER (2013)[32]. There are some factors that influence diffusion and depends on both the diffusing host component and the temperature, this diffusion coefficient being a function of temperature. In semiconductors, heat treatments promote the diffusion of impurities that are transported into the host cell and it may also occur that such transport carries these impurities further into the host cell, generating a more suitable concentration distribution.

The diffracto grams show formation of the TTB structure with monophasic and crystalline characteristics even with doping's made with the nickel metal forming the system $KSr_2(Ni_xNb_{5-x})O_{15-\delta}$ where x varies its doping, x = 0,25; 0,50 and 0,75. The calcination at 1250 ° C, the grains present expansion evidenced in the diffracto graphic peaks exposed in Figure 2, where these peaks are pointed and narrow, what causes the system to present crystallinity and to be monophasic. This process favors the absence or even decrease (elimination) of defects found in the crystalline lattice due solely to structural homogeneity. By means of this phase

expansion, we have an increase in crystallinity, which can be evidenced by decreasing the width of the diffraction peaks, increasing in intensity and in numbers. The diffracto gram (Figure 2) shows the formation of the phase with structure of tetragonal symmetry (TB). With the thermal treatment of the precursor powder performed at 1250 ° C / 1h the values of the interplanar distances, relative intensity and $2\boldsymbol{\theta}$ of the experimental diffracto gram coincide with the crystallographic JCPDS_34-0108 (2000)[27], this sheet refers to the phase of $KSr_2Nb_5O_{15}$. No other secondary phase has been identified, showing that the compound obtained is monophasic. For solid solutions with $x \leq 0,75$ diffracto grams showed the formation of a single phase associated with $KSr_2Nb_5O_{15}$.

The valence of the Ni^{2+} in solid solutions of $KSr_2(Ni_xNb_{5-x})O_{15-\delta}$, since the oxidation state 3+ of the nickel (Ni) cation has been rarely detected. The substitution of cations of large radius (r) such as, for example, Sr^{2+} (r_{Sr}^{2+} = 1,18 Å) by cations of small radius (r), such as Ni^{2+} (r_{Ni}^{2+} = 0,69 Å) not favorable. In addition, the cations of Ni^{2+} show strong preference for octahedral coordination, the same coordination of niobium (Nb). In this sense, the ionic radius of Nb cations in a high oxidation state (r_{Nb}^{5+} = 0,64 Å), similarity with the ionic radius of the Ni^{2+}. However, the valence difference is equal to three units, which is not favorable. However, the best similarity of the ionic Ni^{2+} occurs for the Nb^{5+} partially reduced to Nb^{4+} (r_{Nb}^{4+} = 0,68 Å). Here it is important to note that the Nb4 + represents a partial reduction of the niobium cation, whereas a completely reduced state is given by the niobium with valence 3+, Nb^{3+}, (r_{Nb}^{3+} = 0,72 Å); LANFREDI et al. (2005)[26]. The considerable increase in the network parameters may be associated with the partial substitution of ions Nb^{5+} by the ions Ni^{2+} in the crystalline lattice, where there is a decrease in the covalent character of the bond Nb-O with the increase in the ionic character of the bond Ni-O; LANFREDI et al. (2015)[33]. In fact, the results of the FT-IR (Fig. 1) showed a correlation between the wave number of the bands and the displacement magnitude of the decentralized Nb location as a function of the increased doping of the powders $KSr_2Nb_5O_{15}$; LANFREDI, FOLGUERAS-DOMÍNGUES, RODRIGUES (1995)[25]. The partial replacement of niobium cations by nickel cations in the host structure can be accompanied by the formation of oxygen vacancies from the charge compensation mechanism due to the partial reduction of niobium; LANFREDI et al. (2015)[33]. Thus, the formation of oxygen vacancies can be accompanied by disproportionation of cations Nb^{5+} for Nb^{3+}, in which it presents a larger ionic value due to its punctual loading, where $r_{Nb}^{3+} > r_{Ni}^{2+} > r_{Nb}^{5+}$, thus justifying the decrease in the volume value of the unit cell. Furthermore, nickel cations specifically occupy the position of the Nb(1). This may be due to the ion ray value and the preferential octahedron occupation. This occupation results in a degree of distortion of the octahedron of the $[Nb(2)O_6]$, where this distortion is necessary for an accommodation of the nickel cations to occur in the formation of the structure.

In the host structure $KSr_2Nb_5O_{15}$, the niobium has preference in occupying the octahedral sites, NbO_6. Cation substitution Nb^{5+} by cations Ni^{2+} can cause distortions in the octahedra as well as the creation of a sub level of energy resulting from the formation of gaps due to the difference of electrons between the cation Nb^{5+} and doping cation, resulting in a decrease in the band gap. A higher degree of distortion and structural defects can be expected as a result of increased nickel doping. However, doping with 0.75 mol of Nickel can cause such a disorder, in such a way that the electronic mobility of the electrons is hampered, requiring a greater energy for electronic transitions of the conduction band to the valence band.

In terms of the first-order apparent rate, it should be noted that all niobate-based materials presented less photo activity when compared to TiO_2. The conversion of Basic Blue 41 is probably attributed to a series of chemical reactions occurring on the outer surface of these doped Nb-based materials Ni^{2+}. Thus, a deeper analysis of the photo catalytic activity can be performed to obtain the overall reaction rate considering the surface concentration of Basic Blue 41, since this primary fraction of Basic Blue 41 molecules will undergo photo degradation. The photo catalytic degradation of Basic Blue 41 can be considered as a unimolecular catalytic surface reaction, where the adsorption of Basic Blue 41 followed by photo degradation under irradiation UV; ATAR, OLGUN, ÇOLAK (2008)[1]. The reaction rate for the degradation of Basic Blue 41 was faster for photo catalysts with $KSr_2(Ni_xNb_{5-x})O_{15-\delta}$ where x = 0,50 ($KSNNi_{0,50}$). These results suggest that changes in the crystalline structure of the niobate-based material, especially when increased binding occurs Nb-O(6) can notably influence photo catalytic activity. Probably, it is the most active oxygen in the sense of probability of the transfer of charge to the molecules of O_2 and therefore the longer the length of such a connection Nb-O the more this distortion occurs, and thus the greater the efficiency of electron transfer and the greater the photo catalytic activity. Otherwise, it can serve as a more active center, a trap; JUAN, JORGE, JEAN-MARIE (2001)[34] and JUAN, JORGE, JEAN-MARIE (1998)[35][34-35] on the nature of the dominant species of reactive oxygen.

V. Conclusões

The chemical synthesis based on the modified Polyol method proved to be adequate for the preparation of monophasic and crystalline post-

$KSr_2(Ni_xNb_{5-x})O_{15-\delta}$, where x = 0,25; 0,5 and 0,75 with stoichiometry can be controlled. In addition, the production of the post-ceramics with a shorter calcination time than those prepared by conventional mixing of oxides. Due to the high polarity of the polyols, the inorganic salts (precursors) are easily solubilized; The nucleation and growth steps occur at the boiling point of the polyalcohol (eg, ethylene glycol at 197 ° C, diethyleneglycol at 246 ° C and tetraethyleneglycol at 314 ° C) and the use of high temperatures (at the boiling point of the polyalcohol) produces materials with high crystallinity;

Absorption spectroscopy in the infrared region showed a displacement of the bands characteristic of the Nb-O for regions of low frequencies with increasing concentration of nickel cations. This displacement shows that the bonds between niobium and oxygen cations, for the nickel doped solid solutions, are shorter than $KSr_2Nb_5O_{15}$;

The lines of the crystal, JCPDS: 34-0108 (2000)[27], coincides with the peaks of the diffracto gram, however it is noticed a singular difference of these peaks, relative intensity has lower intensity (figure 2 – c) $KSNNI_{0,75}$) in relation to the relative intensity of $KSNNI_{0,50}$ in Figure 2, where in this diffracto gram the intensity of the peaks is much more expressive and defined, but narrower and sharper, which demonstrated in descending order of relative intensities $I_{R(KSNNi\mathbf{0,50})} > I_{R(KSNNI\mathbf{0,25})} > I_{R(KSNNI\mathbf{0,75})}$;

A decrease of the absorbance values as a function of time was observed for the concentration of the basic blue 41 dye in solution, resulting from the photo degradation of the photo catalytic tests performed for the photo catalyst $KSNNi_{0,50}$ which presented lower absorbance value.

References Références Referencias

1. NECIP Atar, ASIM Olgun, FERDAĞ Çolak. Thermodynamic, Equilibrium and Kinetic Study of the Biosorption of Basic Blue 41 using *Bacillus macerans. Eng. Life Sci.* 2008, v. *8*, n. 5, p. 499–506.
2. LUCIANO EVANGELISTA Fraga, MARIA VOLNICE BOLDRIN Zanoni. Photoelectrocatalytical degradation of basic blue 41 dye usingnanoporous semiconductor of Ti/TiO2. Eclética Química. 2009, V. 34, n. 4, 27-36.
3. ZHANG Gaoke, LI Yiqiu, WANG Junting, TU Haibin, YU Xinyi. Characterization and Photocatalytic Activity of $KSr_2Nb_5O_{15}$ with Tungsten Bronze Structure [J]. J. Wuhan Univ.of Tech-Mater. Sci. Ed., 2009, 24(5): 742-746.
4. MATOS Juan, LANFREDI Silvania, MONTANA Ricmary, AUGUSTO LIMA NOBRE Marcos, FERNÁNDEZ ÓRDOBA María, ANIA Conchi. Photochemical reactivity of apical oxygen in $KSr_2Nb_5O_{15}$ materials for environmental remediation under UV irradiation. J. of Coll. and Interf. Sci., 2017, 496, 211–221.
5. LI, C., CAI, W., CAO, B., SUN, F., LI, Y., KAN, C., ZHANG, L., Mass Synthesis of Large, Single-Crystal Au Nanosheets Based on a Polyol Process ,Adv. Funct. Mater., 16, 83–90, (2006).
6. CLAUS Feldman. Polyol - Mediated Synthesis of Nanoscale Functional Materials, Solid State Science, v. 7, p. 868-873, 2005.
7. SINGARAVELU Vivekananghan, VENKATESWARLU Manne, SATYANARAYANA, N. Effect of Ethylene Glycol on Polyacrylic Acid based Combustion Process for the Synthesis of Nano-cristalline Nickel Ferrite (NiFe2O4), Materials Letters, v. 58, p. 2717-2720, 2004.
8. YEBIN Xu, GUOHUA Huang, HUA Longo. Synthesis of Lanthanum Aluminate via the Ethylenediaminetetraacetic Acid Gel Route, Ceramics International, v. 29, p. 837-840, 2003.
9. YUGANG Sun, YADONG Yin, BRAIAN T Mayers, THURSTON Herricks, YOUNAN Xia. Uniform Silver Nanowires Synthesis by Reducing AgNO3 with Ethylene Glycol in the Presence of Seeds and Poly (vinyl pyrrolidone), Chemistry of Materials, v. 14, n. 11, p. 4736-4745, 2002.
10. SILVANIA Lanfredi, GUSTAVO Palacio, FELIPE SILVA Bellucci, CLAIRE V Colin, MARCOS ANTONIO L. Nobre, Thermistor behaviour and electric conduction analysis of Ni-doped niobate ferroelectric: the role of multiple β parameters, *Journal of Physics D: Applied Physics*, 2012, 45, 435302.
11. DANTAS, S. A.; SILVANIA Lanfredi, MARCOS AUGUSTO L. Nobre, Crystallographic Properties of $Sr_2NaNb_5O_{15}$ Synthesized by Modified Polyol Method. Journal of Physics D; Applied Physics, 2012, 45 (43), 139-143.
12. JULIO Bregado-Gutierrez, ARMANDO J. Saldivar-Garcia, HUGO F. Lopez. Synthesis of Silver Nanocrystals by a Modified Polyol Method. Journal of Applied Polymer Science., 2008, 107 (1), 45–53.
13. SILVANIA Lanfredi, FELIPE SILVA Bellucci, CLAIRE V Colin, MARCOS ANTONIO L. Nobre. Phase transitions and interface phenomena in the cryogenic temperature domain of a niobate nanostructured ceramic, *Dalton Trans*actions., 2014, 43, 10983-10998.
14. CHU-YUN Hsiao, WEI-MIN Li, KUO-SHIN Tung, CHUAN-FENG Shih, WEN-DUNG Hsu. Synthesis and application of magnesium oxide nanospheres with high surface area, Materials Research Bulletin, 2012, 47 (11), 3912-3915.
15. SILVANIA Lanfredi, DIEGO H. M Gênova, IARA A. O. Brito, ALAM R. F. Lima, MARCOS A. L. NOBRE. Structural characterization and Curie temperature

determination of a sodium strontium niobate ferroelectric nanostructured powder. Journal of Solid State Chemistry, 2011, 184 (5), 990-1000.
16. MARCOS A. L. Nobre, SILVANIA, Lanfredi. Electrical characterization by impedance spectroscopy of Zn7Sb2O12 ceramic. Materials Research, 2003, 6 (2), 151-156.
17. MARCOS A. L. Nobre, Estudo da formação de fases no sistema ZnO.Sb2O3 por síntese química e efeito de cátions de metais de transição sobre a cristalinidade. PhD Dissertação (Mestrado em Química) – Centro de Ciências Exatas e Tecnologia, Universidade Federal de São Carlos, São Carlos. 1995: 165.
18. MARCOS A. L. Nobre. Varistores a Base de ZnO Obtidos a Partir das Fases ZnSb2O6 e Zn7Sb2O12: Correlação entre as Fases, Microestrutura e Propriedades Elétricas. Tese (Doutorado em Ciências) – Centro de Ciências Exatas e Tecnologia, Universidade Federal de São Carlos, São Carlos. 1999. 203.
19. MAGGIO P. Pechini. U.S. Patent, 1967, No. 3.330.697.
20. SILVANIA Lanfredi, MARCOS A. L. Nobre, PAULA G. P. Moraes, JUAN Matos. Photodegradation of phenol red on a Ni-doped niobate/carbon composite, *Ceramics International*, 2014, 40 (7), 9525-9534.
21. NUFFIELD, E. W. X-ray diffration methods. *New York: John Wiley & Sons*, p.147, (1986).
22. DENIO Silva, NITO Debacher, ARMANDO Castilho Jr., FABIO Rohers. Caracterização Físico-Química e Microestrutural de Conchas de Moluscos Bivalves Provenientes de Cultivos da Região Litorânea da Ilha de Santa Catarina; Quim. Nova., 2010, 33 (5), 1053-1058.
23. YEBIN Xu, GUOHUA Huang, HUA Longo. Synthesis of Lanthanum Aluminate via the Ethylenedia minete traacetic Acid Gel Route, Ceramics International., 2003, 29 (7), 837-840.
24. VANDERLEI S. Bergamaschi. Influência de Parâmetros de Precipitação nas Características Físicas e Químicas do Carbonato de Zircônio; Dissertação (Mestrado), Mestre em Ciências na Área de Tecnologia Nuclear- Materiais – IPEN, São Paulo, 2000.
25. SILVANIA Lanfredi, SILVIO Folgueras-Domingues, ANA C. M. Rodrigues. Preparation of LiNbO3 Powder from the Thermal Decomposition of a Precursor Salt Obtained by an Evaporative Method. J. Mater. Chem. v. 5, p. 1995, 1995.
26. SILVANIA Lanfredi, LUIS R. Trindade, ANTONIO R Barros, NILTON Feitosa, MARCOS A. L. Nobre. Síntese e Caracterização Estrutural do Niobato de Potássio e Estrôncio com Estrutura tipo Tetragonal Tungstênio Bronze TTB, Cerâmica, 51, 151, (2005).
27. JCPDS – International Centre for Diffraction Data. PCPDFWIN v. 2.1. Copyright© JCPDS-ICDD. 2000.
28. LEONIDE Azaroff, MARTIN J. Buerguer. The Powder Method in X-Ray Crystallography, McGraw-Hill, 1958.
29. MELO, D., S..; Pigmentos pretos a base de Cobaltitas de Lantânio. Dissertação (Mestrado em Química) Departamento de Química - Centro de Ciências Exatas e da Natureza de João Pessoa – PB. Universidade Federal da Paraíba, João Pessoa. 2007. 98.
30. DANTAS, S., A.; LIMA, A., R., F.; MARCOS A. L. Nobre, SILVANIA Lanfredi. Análise Cristalográfica e Efeito da Dopagem com Cátios Ferro Sobre a Ceramica $Sr_2Na(FeNb_4)O_{15-\delta}$ com Estrutura Tetragonal Tungstênio Bronze. Anais do 53° Congresso Brasileiro de Cerâmica, Guarujá – SP, 2009.
31. CHUNJIE Wang, YUE Wang, WENZHI Huang, BINGLIN Zou, ZUAHIR S. Khan, YU Zhao, JILI Yang, XUEQIANG Cao. Influence of CeO_2 addition on crystal growth behavior of CeO_2–Y_2O_3–ZrO_2 solid solution. Ceramics International 38, 2087–2094, (2012).
32. WILLIAN D. Callister, DAVID G. Rethwish. Ciencias e Engenharia de Materiais Uma Introdução 8ª ed. 2013, 105-121.
33. SILVANIA Lanfredi et al. Spectral Deconvolution as a Tool to Understanding Curie-Temperature Shifting and Niobium Off-Centering Phenomenon in Ferroelectrics of Type Niobates. Applied Mathematical Sciences., 2015, 9 (117), 5839 – 5869.
34. JUAN Matos, JORGE Laine, JEAN-MARIE Herrmann, Synergy effect in the photo catalytic degradation of phenol on a suspended mixture of titania and activated carbon, Appl. Catal. B: Environ., 1998, 18 (3-4) 281–291.
35. JUAN Matos, JORGE Laine, JEAN-MARIE Herrmann, Effect of the type of activated carbons on the photo catalytic degradation of aqueous organic pollutants by UV-Irradiated titania, J. Catal., 2001, 200 (1) 10–20.